CRYSTAL GROWTH & DESIGN
2007
VOL. 7, NO. 10
1988−1991

Controlled Growth and Optical Properties of One-Dimensional ZnO Nanostructures on SnO_2 Nanobelts

Shuhui Sun,*[,†,§] Guowen Meng,*[,†] Gaixia Zhang,[‡] and Lide Zhang[†]

Key Laboratory of Materials Physics, and Anhui Key Laboratory of Nanomaterials and Nanostructures, Institute of Solid State Physics, Chinese Academy of Sciences, Hefei 230031, P. R. China, and Département de Génie Physique, École Polytechnique, Montréal H3C 3A7, Canada

Received February 21, 2007; Revised Manuscript Received April 23, 2007

ABSTRACT: Various ZnO nanostructures, such as nanobelts, nanorods, and nanowires, have been grown on presynthesized SnO_2 nanobelts via a simple thermal evaporation of Zn powders, without using any catalysts, producing various heterostructures. The evaporation temperature is the critical experimental parameter for the formation of different morphologies of these nanostructures. Room-temperature photoluminescence spectra of the heterostructures show that the relative intensity of ultraviolet emission to the green band can be tuned by controlling the morphologies and sizes of the secondary-grown 1D ZnO nanostructures, suggesting that the nano-heterostructures of these nanostructures grown on SnO_2 nanobelts may have potential applications in nano-optoelectronic devices.

1. Introduction

One-dimensional (1D) nanostructures, such as nanotubes, nanowires, nanorods, and nanobelts are attractive building blocks for the "bottom-up" assembly of electronic and optoelectronic device systems, such as sensors, laser diodes, field-effect transistors, and light-emitting diodes because of their interesting geometries and unique physical and chemical properties.[1] To date, much effort has been focused on the integration of 1D nanoscale building blocks into two- and three-dimensional (2D, 3D) ordered superstructures or complex functional architectures, which is a crucial step toward the realization of functional nanoscale systems.[2] ZnO branched nanowire and nanoribbon junction arrays have been synthesized by thermal evaporation.[3] More complex structures, such as MgO fishbones,[4] SiOx novel nanostructures,[5] ZnO junction arrays,[6] and SnO networks,[7] have also been reported. Hierarchical nanostructures, in which the primary stems (or trunks) and the branches consisting of either the same or different materials, offer another approach for increasing structural complexity and enabling greater function. Various hierarchical nanostructures, such as ZnO,[8] In_2O_3,[9] Pb−Se,[10] Si−SiO_2,[11a,b] W−WO_3,[11c] and ZnS−CdS[11d] have been achieved by various gas-phase growth methods. The ability to control the morphology, size, and composition of the building blocks of hierarchical nanostructures in a predictable manner during synthesis and, therefore, to modulate their properties is very important for the realization of multifunctional nanodevices. Although 1D nanostructures of ZnO and SnO_2 have been studied extensively, few studies of ZnO−SnO_2 hetero-nanostructures have been reported. In this letter, we report the morphology-controlled synthesis of ZnO nanobelts/nanorods/nanowires grown on SnO_2 nanobelt substrates, forming various hetero-nanostructures via a simple thermal evaporation and condensation method without catalyst, which permits the modulation of their optical properties. These heterostructures may have potential applications in optoelectronic nanodevices.

2. Experimental Section

The morphology-controlled heterojunctions of 1D ZnO nanostructures on SnO_2 nanobelt were achieved by a simple two-step vapor-solid (VS) process. The first step was the growth of SnO_2 nanobelts to serve as substrates (stems or trunks) for the secondary growth. The second step was to grow 1D ZnO nanobranches on these substrates. Both synthesis processes were performed in a quartz tube (inner diameter ca. 30 mm; length ca. 1200 mm) inserted inside a horizontal high-temperature furnace. The synthesis of single-crystal SnO_2 nanobelts substrates was described in detail in our previous work.[12] For the second-step growth, zinc powder (purity >90%) was put in one end of an alumina boat. The presynthesized SnO_2 nanobelts were put at the downstream in the same boat, acting as the substrates to grow ZnO nanostructures. The boat was placed in the central region of the quartz tube, heated to 800 °C at a heating rate of 15 °C/min, kept at this temperature for 1 h, and subsequently cooled down to room temperature. A total Ar flow rate of 100 sccm was maintained throughout the experiment.

The as-synthesized heterojunction nanostructures were studied by X-ray diffraction (XRD, X'Pert Pro MPD), scanning electron microscopy (SEM, JEOL JSM 6700F at 10 kV) equipped with energy-dispersive X-ray spectroscopy (EDS), and high-resolution transmission electron microscopy (HRTEM, JEOL 2010 at 200 kV). The photoluminescence (PL) spectrum was measured at room temperature with an Edinburgh luminescence spectrometer (FLS 920), using a 325 nm xenon lamp as the excitation source. X-ray photoelectron spectroscopic (XPS) analysis was carried out in a VG ESCALAB 220iXL, using a monochromatic Al Kα source (1486.6 eV), at a base pressure $<10^{-10}$ Torr. All the binding energies were calibrated by the C1s line of adventitious hydrocarbon at 284.4 eV. After Shirley background removal, the component peaks were separated using the freely available XPSPeak fitting program, version 4.1.

3. Results and Discussion

Figure 1 shows the typical SEM images of (a) the primary SnO_2 nanobelts before secondary growth and (b) the secondary-grown 1D ZnO nanostructures on the primary SnO_2 nanobelt substrates synthesized at 800 °C. Figure 1a shows the beltlike geographic shape of pristine SnO_2 substrate. Their widths are from several hundreds nanometers to several micrometers, and lengths are up to millimeter scale. It is clearly seen (Figure 1b) that a high density of well-aligned ZnO nanobelts have been grown on the SnO_2 nanobelt surface. The coverage of these secondary-grown nanobelts appears to be quite uniform. Most secondary-grown nanobelts do not have a uniform width; they

* To whom correspondence should be addressed. E-mail: shsuncn@hotmail.com; gwmeng@issp.ac.cn.
† Chinese Academy of Sciences.
‡ École Polytechnique.
§ Present address: INRS-EMT, 1650 boulevard Lionel Boulet, Varennes, Quebec, Canada J3X 1S2.

10.1021/cg0701776 CCC: $37.00
Published on Web 09/14/2007

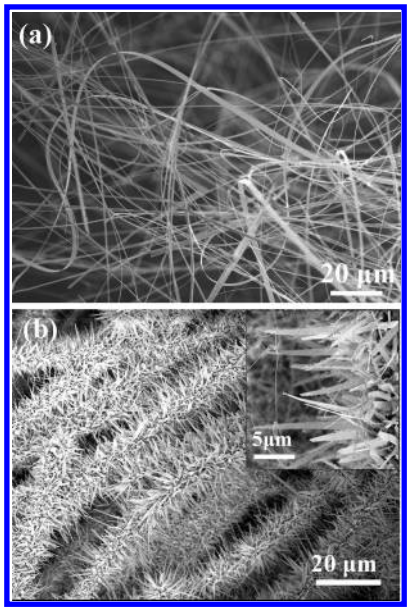

Figure 1. (a) SEM image of the primary SnO_2 nanobelts before secondary growth; (b) SEM image of secondary−grown ZnO nanobelts on the primary SnO_2 nanobelt.

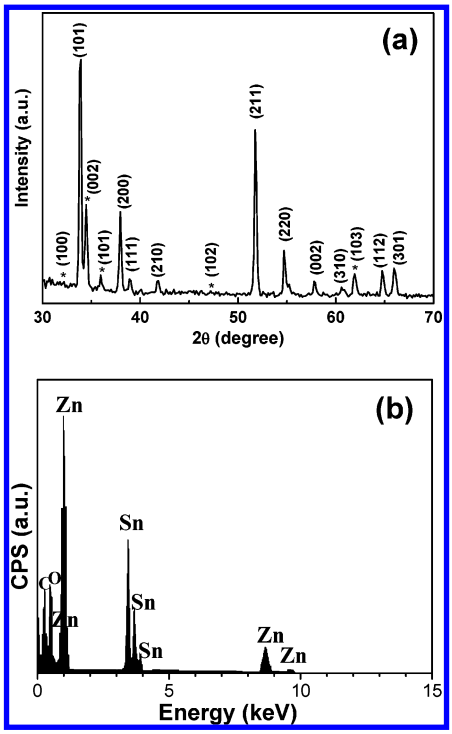

Figure 2. (a) XRD patterns (∗ represents ZnO peaks), and (b) EDS of ZnO−SnO_2 hierarchical nanostructures.

become thinner toward the tip, forming a sharp edge. From the enlarged view in the inset of Figure 1b, it can be seen that the nanobelts are 500−800 nm wide at the root, and 5−20 μm long. Figure 2a shows the XRD pattern obtained from the ZnO−SnO_2 heterostructures, indicating that both the secondary-grown ZnO nanobelt branches and the primary SnO_2 nanobelt substrates are highly crystallized. All the diffraction peaks can be indexed to be wurtzite ZnO and tetragonal rutile SnO_2; no other crystalline forms are detected. The EDS spectrum in Figure 2b demonstrates the purity of the sample; only zinc, tin, and oxygen are detected.

The chemical state and purity of the hierarchical nanostructures were studied by XPS analysis. As shown in Figure 3, both Sn $3d_{5/2}$ and Zn $2p_{3/2}$ high-resolution spectra, showing essentially symmetric lineshapes, are fitted by single components, with binding energies at 486.7 and 1022.2 eV, respectively, which are assigned to Sn^{4+} in SnO_2[13] and Zn^{2+} in ZnO.[14] No obvious shoulders representing any other chemical states of Sn and Zn were found. This indicates the purity of the SnO_2 and ZnO produced. Their binding energies are slightly higher, and their full-widths at half-maxima (fwhm) are slightly broader than those of bulk materials, which may be due to size effects[15] and their slight mixing. XPS is a very useful analytical technique for quantifying the atomic composition. Thus, for these hierarchical nanostructures, we obtained the relative atomic concentration Zn/Sn ratio of 22:1, as determined from our experimental XPS peak areas and their relative sensitivity factors, indicating that large quantities of ZnO nanostructures have grown on the primary SnO_2 nanobelt surfaces. The O1s spectrum is located at 531.2 eV; it is symmetric and appears to have no components at higher binding energies. This is the region attributable to inorganic oxides, such as the SnO_2 and ZnO that we are discussing. We make no attempt to separate them here.

TEM was used to investigate the microstructure of the ZnO−SnO_2 heterojunctions in more detail. Figure 4a shows the representative morphology of the ZnO nanobelt branches grown from the primary SnO_2 nanobelt substrate, where the primary SnO_2 nanobelt stem appears comparatively dark, owing to its thickness. The bright field TEM image clearly shows that well-aligned ZnO branches grow nearly perpendicular to the primary nanobelt substrate. It should be noted that, because of sonication during the TEM sample preparation process, some branches were broken off from the stem. Some broken branches can be observed in Figure 4a. In addition, the different brightness contrast of the branches reveals different levels of them. Figure 4b shows the high-resolution TEM image of the ZnO branch, and the inset is the corresponding fast Fourier transform (FFT) of the image. The lattice fringe spacing of the ZnO nanobranch is 0.52 nm, corresponding to the (0001) fringe perpendicular to the growth direction, being consistent with that of the bulk wurtzite ZnO crystal.

By tuning the growth temperatures, the secondary-grown 1D ZnO nanostructures on the primary SnO_2 nanobelt stem, with different shapes and sizes, can be well controlled. Figure 5 panels a and b, respectively, show the SEM images of the secondary ZnO nanostructures grown on the primary SnO_2 nanobelt substrates at 450 and 600 °C. At low-growth temperature (450 °C), well-aligned secondary ZnO nanowires grow on the surfaces of the primary SnO_2 nanobelt substrates, as shown in Figure 5a and its inset. The diameters of the secondary-grown ZnO nanowires normally range from 30−50 nm and their lengths are several micrometers. When the growth temperature was increased to 600 °C, ZnO nanorods, with hexagonal cross sections, are formed on the nanobelt substrates (see Figure 5b). The nanorods have diameters of 100−300 nm and lengths of 400 nm−3 μm. The white arrow indicates the SnO_2 nanobelt stem, which acts as the substrate for the secondary growth of 1D ZnO nanostructures. SEM results reveal that there are no nanoparticles observed on any tips of the secondary-grown ZnO nanostructures. Because the only source material used in our synthesis was zinc powders, it is likely that the growth of secondary-grown ZnO nanostructures is governed by the vapor−solid (VS) mechanism;[16] that is, Zn vapor, evaporated from the starting material, oxidized and deposited on a SnO_2 nanobelt

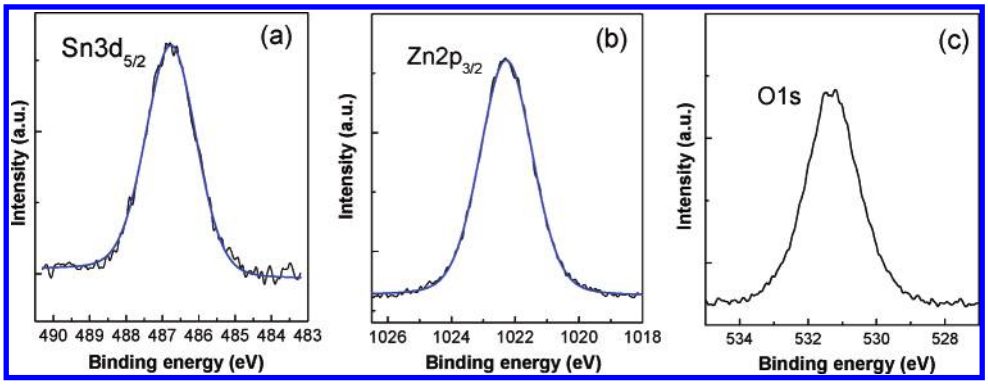

Figure 3. XPS spectra of ZnO−SnO_2 hierarchical nanostructures: (a) Sn $3d_{5/2}$, (b) Zn $2p_{3/2}$, and (c) O1s spectra, respectively.

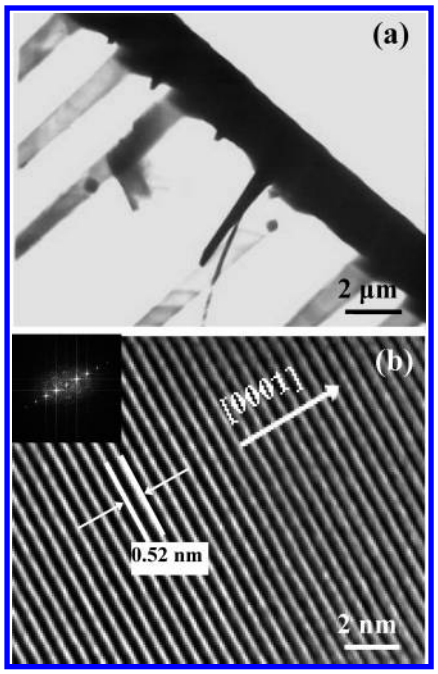

Figure 4. (a) TEM image of ZnO−SnO_2 hierarchical nanostructures and (b) HRTEM image of a representative ZnO nanobranch. The inset is the corresponding fast Fourier transform of the image.

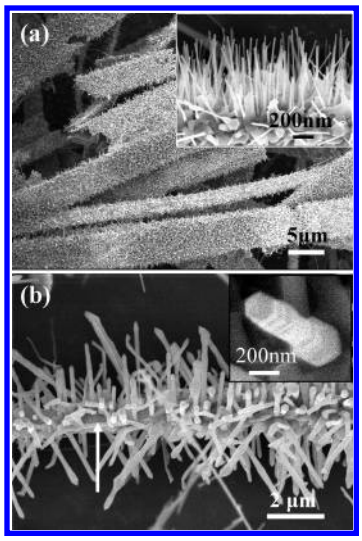

Figure 5. SEM images of the secondary-grown ZnO nanostructures on the primary SnO_2 nanobelt substrate at (a) 450 °C and (b) 650 °C.

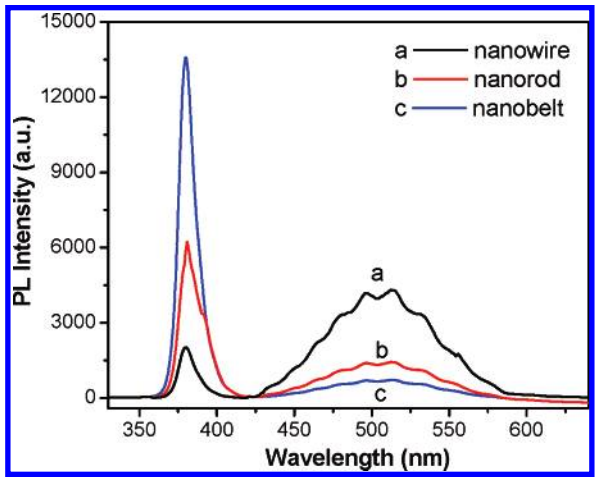

Figure 6. Panels a, b, and c show the room-temperature PL spectra of the products corresponding to the ZnO nanostructures synthesized at 450, 650, and 800 °C, respectively.

substrate and grew into various nanostructures. It is generally believed that the growth temperature and gas-phase supersaturation determine the growth rate of surface planes and the final morphology of the crystals. Higher temperatures favor the growth of ZnO nanobelts, while ZnO nanowires are formed at relatively low temperature.[17,18]

The corresponding PL spectra, recorded from the secondary-grown ZnO nanowires, nanorods, and nanobelts on the primary SnO_2 nanobelt substrate, are shown, respectively, in panels a, b, and c of Figure 6. The PL from only the secondary-grown ZnO nanostructures, not the SnO_2 nanobelts, was observed, which may due to the high-density coverage of ZnO on SnO_2 substrates. All spectra are composed of a relatively sharp ultraviolet (UV) emission centered at ∼380 nm and a broad green emission centered at ∼510 nm. It is generally accepted that the UV emission of ZnO is attributed to free-exciton recombination at the near-band edge, while the deep-level green emission of ZnO is due to the radiative recombination of the photogenerated holes with electrons belonging to the oxygen vacancy of the surface.[19] Dijken et al. have proposed that, upon photon excitation, the valence band holes that are created can be trapped by the surface states and then tunnel back into one-electron oxygen vacancies (V_o^*) to form a V_o^{**} recombination center, leading to the visible emission by the recombination between a shallowly trapped electron and a deeply trapped hole in a V_o^{**} center.[20] It has been suggested that high crystallinity (decrease of impurity and structural defects such as oxygen vacancy, dislocations, etc.) and the diameter of the nanowires,

obtained at high temperature, play a key role in the enhancement of the UV emission.[21,22] Similar work has also been reported by Yang[23] and Yao[24] in which the strong UV emission from thicker ZnO nanowires is suggested to be due to the low concentration of oxygen vacancies. As clearly shown in Figure 6, the progressive increasing ratio of the green-light emission over UV peak intensity as the size of the ZnO nanostructure decreases from nanobelt to nanorod to nanowire suggests that there is a greater fraction of oxygen vacancies in the thinner ZnO nanostructure branches. We believe that the higher surface-to-volume ratio for thinner ZnO nanostructures favors a higher level of surface and subsurface oxygen vacancies. In addition, since thinner ZnO nanostructures grow under the low temperature, the point defect density in ZnO crystals should be higher than those grown under high temperature.[24] We suggest that all these factors possibly cause the increase of the green-band emission. Thus, the optical properties could be modulated by tuning the growth temperatures of ZnO nanostructures.

4. Conclusion

In summary, we have described the secondary growth of highly crystalline ZnO nanostructures on primary SnO_2 nanobelt substrates via a simple thermal evaporation and condensation method. It was found that by tuning the growth temperature and in the absence of catalysts, sharp nanobelts, nanorods, and thin nanowires of ZnO could form on the primary SnO_2 nanobelt, and correspondingly, their optical properties could be modulated. This suggests a simple method of making heterojunctions between nanobelts and nanowires for nanodevices. We believe that these ZnO−SnO_2 heterojunction nanostructures have potential in nanoscale optoelectronic devices.

Acknowledgment. This work was supported by the National Science Fund for Distinguished Young Scholars (Grant No. 50525207), the Natural Science Foundation of China (Grant No. 10374092), the Knowledge Innovation Program of the Chinese Academy of Sciences (Grant No. KJCX2-SW-W31), and the National Basic Research Program of China (Grant No. 2007CB936601).

References

(1) (a) Jiang, Y.; Zhang, W. J.; Jie, J. S.; Meng, X. M.; Zapien, J. A.; Lee, S. T. *Adv. Mater.* **2006**, *18*, 1527. (b) Lieber, C. M. *MRS Bull.* **2003**, *28*, 486. (c) Xia, Y.; Yang, P.; Sun, Y.; Mayers, B.; Gate, B.; Yin, Y.; Kim, F.; Yan, H. *Adv. Mater.* **2003**, *15*, 353. (d) Huang, M. H.; Mao, S.; Feick, H.; Yan, H.; Wu, Y.; Kind, H.; Webber, E.; Russo, R.; Yang, P. *Science*, **2001**, *292*, 1897. (e) Kim, M. H.; Cho, Y. H.; Lee, H.; II Kim, S.; Ryu, S. R.; Kim, D. Y.; Kang, T. W.; Chung, K. S. *Nano Lett.* **2004**, *4*, 1059.

(2) Gudiksen, M. S.; Lauhon, L. J.; Wang, J. F.; Smith, D. C.; Lieber, C. M. *Nature* (*London*) **2002**, *415*, 617.

(3) Gao, P.; Wang, Z. L. *J. Phys. Chem. B* **2002**, *106*, 12653.

(4) Zhu, Y. Q.; Hsu, W. K.; Zhou, W. Z.; Terrones, M.; Kroto, H. W.; Walton, D. R. M. *Chem. Phys. Lett.* **2001**, *347*, 337.

(5) Sun, S. H.; Meng, G. W.; Zhang, M. G.; Hao, Y. F.; Zhang, X. R.; Zhang, L. D. *J. Phys. Chem. B* **2003**, *107*, 13029.

(6) Gao, T.; Wang, T. H. *J. Nanosci. Nanotechnol.* **2005**, *9*, 1120.

(7) Kim, H.; Sigmund, W. *Appl. Phys. Lett.* **2002**, *81*, 2085.

(8) Lao, J. Y.; Wen, J. G.; Ren, Z. F. *Nano Lett.* **2002**, *2*, 1287.

(9) Wen, J. G.; Lao, J. Y.; Wang, D. Z.; Kyaw, T. M.; Foo, Y. L.; Ren, Z. F. *Chem. Phys. Lett.* **2003**, *372*, 717.

(10) Poudel, B.; Wang, W. Z.; Wang, D. Z.; Huang, J. Y.; Ren, Z. F. *J. Nanosci. Nanotechnol.* **2006**, *6*, 1050.

(11) (a) Ye, C. H.; Zhang, L. D.; Fang, X. S.; Wang, Y. H.; Yan, P.; Zhao, J. W. *Adv. Mater.* **2004**, *16*, 1019. (b) Hu, J.; Bando, Y.; Zhan, J.; Yuan, X.; Sekiguchi, T.; Golberg, D. *Adv. Mater.* **2005**, *17*, 971. (c) Baek, Y.; Song, Y.; Yong, K. *Adv. Mater.* **2006**, *18*, 3105. (d) Jung, Y.; Ko, D. K.; Agarwal, R. *Nano. Lett.* **2007**, *7*, 264.

(12) Sun, S. H.; Meng, G. W.; Wang, Y. W.; Gao, T.; Zhang, M. G.; Tian, Y. T.; Peng, X. S.; Zhang, L. D. *Appl. Phys. A* **2003**, *76*, 287.

(13) NIST X-ray Photoelectron Spectroscopy Database. http://srdata.nist.gov/xps, accessed November 2006.

(14) Liu, J. W.; Li, X. J.; Dai, L. M. *Adv. Mater.* **2006**, *18*, 1740.

(15) Yang, D. Q.; Zhang, G. X.; Sacher, E.; José-Yacamán, M.; Elizondo, N. *J. Phys. Chem. B* **2006**, *110*, 8348.

(16) Pan, Z. W.; Dai, Z. R.; Wang, Z. L. *Science* **2001**, *291*, 1947.

(17) Yao, B. D.; Chan, Y. F.; Wang, N. *Appl. Phys. Lett.* **2002**, *81*, 757.

(18) Ye, C. H.; Fang, X. S.; Hao, Y. F.; Teng, X. M.; Zhang, L. D. *J. Phys. Chem. B* **2005**, *109*, 19758.

(19) Banerjee, D.; Lao, J. Y.; Wang, D. Z.; Huang, J. Y.; Ren, Z. F.; Steeves, D.; Kimball, B.; Sennett, M. *Appl. Phys. Lett.* **2003**, *83*, 2061.

(20) Van Dijken, A.; Meulenkamp, E. A.; Vanmaekelbergh, D.; Meijerink, A. *J. Phys. Chem. B* **2000**, *104*, 1715.

(21) Banerjee. D.; Lao, J. Y.; Wang, D. Z.; Huang, J. Y.; Steeves, D.; Kimball, B.; Ren, Z. F. *Nanotechnology* **2004**, *15*, 404.

(22) Pan, A. L.; Liu, R. B.; Wang, S. Q.; Wu, Z. Y.; Cao, L.; Xie, S. S.; Zou, B. S. *J. Cryst. Growth* **2005**, *282*, 125.

(23) Huang, M. H.; Wu, Y. Y.; Feick, N. T.; Weber, E.; Yang, P. D. *Adv. Mater.* **2001**, *13*, 113.

(24) Yao, B. D.; Chan, Y. F.; Wang, N. *Appl. Phys. Lett.* **2002**, *81*, 757.

CG0701776